The State Scientific Center of Russia
The Budker Institute of Nuclear Physics
SB RAS

V.M. Aulchenko, A.E. Bondar, P. Cantoni,
P.L. Frabetti, S.F. Ganzhur, G.Ya. Kezerashvili,
S.G. Klimenko, F. Lanni, L.A. Leontiev,
B. Maggi, V.M. Malyshev, P.F. Manfredi,
A.L. Maslennikov, A.M. Milov, N.Yu. Muchnoi,
A.P. Onuchin, F. Palombo, V.S. Panin,
S.V. Peleganchuk, Yu.A. Pogorelov, G.E. Pospelov,
I.Ya. Protopopov, V. Re, A. Sala, A.G. Shamov,
D.N. Shatilov, E.A. Simonov, V. Speziali,
L. Stagni, Yu.A. Tikhonov

THE TEST EXPERIMENT WITH THE PROTOTYPE OF LKr CALORIMETER AT THE TAGGED PHOTON BEAM

Budker INP 95-96

НОВОСИБИРСК

The test experiment
with the prototype of LKr calorimeter
at the tagged photon beam

V.M.Aulchenko, A.E.Bondar, S.F.Ganzhur, G.Ya.Kezerashvili,
S.G.Klimenko, L.A.Leontiev, V.M.Malyshev, A.L.Maslennikov,
A.M.Milov, N.Yu.Muchnoi, A.P.Onuchin, V.S.Panin,
S.V.Peleganchuk, Yu.A.Pogorelov, G.E.Pospelov, I.Ya.Protopopov,
A.G.Shamov, D.N.Shatilov, E.A.Simonov, Yu.A.Tikhonov

The State Research Center of Russian Federation
Budker Institute of Nuclear Physics SB RAS
630090, Novosibirsk, Russia

F.Lanni, B.Maggi, F.Palombo, A.Sala
Dipartamento di Fisica dell'Universita' and Sezione INFN,
Milan, Italy

P.Cantoni, P.L.Frabetti, L.Stagni
Dipartamento di Fisica dell'Universita' and Sezione INFN,
Bologna, Italy

P.F.Manfredi, V.Re, V.Speziali
Dipartamento di Electronica Universita' di Pavia and Sezione
INFN, Milan, Italy

Abstract

The experiment with the prototype of liquid krypton electromagnetic calorimeter for *KEDR* detector is described. The experiment was carried out at the *VEPP-4* collider in a tagged photon beam. The tagged photons were obtained in the energy region 50 — 625 *MeV* using the facility *ROKK-1M*. The energy resolution comparable with the resolution of crystal calorimeters and excellent spatial resolution (~1 *mm*) have been obtained. The results are in a good agreement with the Monte Carlo calculation.

1. Introduction

An electromagnetic calorimeter based on liquid krypton is under construction for the *KEDR* detector at the e^+e^- collider *VEPP* − *4M* with a maximum energy of 6 *GeV* [1, 2, 3]. The *LKr* calorimeter gives the energy resolution comparable with *NaI* or *CsI* calorimeters and much better position resolution for photons, due to measuring the photon conversion point. Furthermore the fine granularity of the calorimeter provides information for particle identification based on dE/dx method as well as e/π separation using the shower longitudinal profile.

To investigate the properties of a full absorption calorimeter filled with liquid krypton, we have built two prototypes: prototype–7 (7 *kg* of *LKr*) and prototype–400 (400 *kg* of *LKr*).

The first one was intended to the measurement of the space resolution for charged particles. In the experiment with cosmic particles we have obtained the space resolution $\sigma = 3$ *mm* in the anode readout mode and $\sigma = 0.4$ *mm* in the cathode readout mode for the strips of 10 *mm* width [4]. For the coordinates reconstruction the center of gravity method was used.

To study the energy resolution two experiments with the prototype–400 were performed at the positron beam. The energy resolution 5.7% at 130 *MeV* and 1.9% at 1190 *MeV* have been obtained [4, 5, 6].

The energy and space resolution for high energy electrons (8-80 GeV) were studied by the NA48 collaboration [7].

In this paper we present the new results obtained with the prototype–400 at the tagged photon beam. The energy and space resolution for photons in the wide energy region (50-4500 MeV) have been measured. The present work is also devoted to the test of the final version of electronics for the LKr calorimeter of $KEDR$ detector.

2. The LKr prototype calorimeter

2..1 The prototype design

The prototype calorimeter contains 400 kg of liquid krypton and has the electrode system similar to one of the $KEDR$ calorimeter [5]. In figure 1 the layout of the prototype is shown. The main parameters are listed in table 1, more detailed description of the cryostat and cryogenic system design is published elsewhere [4].

Table 1. Main parameters of the prototype–400.

Gap width	19.5 mm
Electrode thickness	0.5 mm $G10 + 2 \times 18$ μm Cu
Electrode diameter	42 cm
Length of the calorimeter	76 cm ($16.5X_0$)
Number of cells	27
Number of strips	28
Typical cell capacitance	350 pF
Entrance window thickness	$0.13X_0$
Liquid Nitrogen consumption	50 l/day

The electrodes are made of $G10$ sheets covered on the both sides by a copper foil. The first (counting along the photon beam axis) and all odd electrodes are under zero potential ("grounded" electrodes), high voltage is applied to the all even electrodes.

The high voltage electrodes are used for the energy measurements. They are divided into 9 pads centered around the beam axis. Longitudinally the electrode system is segmented in three sections of 6.1 X_0, 5.2 X_0, 5.2 X_0 depth. Thus the calorimeter contains 27 cells for the energy measurements.

The first three "grounded" electrodes are used for the coordinate measurements. They have $8 \div 10$ strips each, parallel to each other. The width of the strips is 1 cm. Some of the "grounded" electrodes are divided into pads

for the cosmic rays trigger. The sketch of the electrode system is shown in figure 2.

2..2 Electronics

The ionization chambers of the calorimeter are operated in the electron-pulse mode. The measurement of the collected charge is provided by the charge sensitive preamplifiers based on FET $NJ1800D$. All the preamplifiers are placed outside the cryostat and connected to the signal electrodes through the two pairs of cold and warm connectors. The preamplifiers are assembled on two motherboards mounted on the warm flange of the cryostat. Each motherboard contains 48 preamplifiers. Each tower or strip is readout by the own preamplifier. The signal from the preamplifier is fed to the RC–$2CR$ shaper by means of a twisted pair of 40 meters long. The amplitudes are digitized by 12–bit analogue-digit converter (ADC) operating in the peak detector mode. To cover the full dynamic range (0.1–4000 MeV) we use two ADC with high and low sensitivity (0.1 MeV/bin and 1 MeV/bin respectively) for each tower channel. The shapers and ADC are located in a special crate $KLUKVA$ [8]. The total number of electronic channels is 96, 41 of them are used for the auxiliary measurements with cosmic rays.

3. Performance of the readout electronics

3..1 Calibration

The important advantages of liquid ionization calorimetry are stability, linearity and uniformity of response that give opportunity for a precision electronic calibration. To exploit this feature in the detector it is necessary to solve two problems:

1. To develop a method of calibration which permits the measurement of relative gain of the readout electronic chain (relative calibration).

2. To measure the parameters of a current signal from particles in the ionization chamber of the calorimeter (absolute calibration).

The relative calibration was performed by injecting a known amount of charge to the preamplifier input through precisely test capacitances C_c (nominal value 6 pF). During the calibration procedure we controlled the pedestal, linearity and the gain of each electronic channel. The calibration coefficients were determined by the linear fit of the channel response to the test pulse.

We used the special designed calibration generator which simulates the shape of a real current pulse. This guarantees an accurate relative calibration of all the channels despite of tolerance of components. For example the difference of the gain constants obtained with the δ and "real" shape calibration signals is shown in figure 3.

The generator consists of the digit-analogue converter (DAC), switches (S1,S2), RC circuit and the integrator (S) (fig. 4). The calibration pulse is generated by switching of the DC signal from the DAC, that results in an exponentially decaying current with the time constant RC flowing into the integrator. The same shape of the current pulse is reproduced at the preamplifier input. The output signal of the integrator is distributed to the preamplifiers by 8 coaxial cables. Each cable serves 12 preamplifiers. The resistors Rm (50 Ω) are used for the cables matching. The calibration signal is computer controlled, which permits an automated calibration and gain equalization procedure.

The calibration capacitances were measured with an accuracy of 0.3%. The nonlinearity of the readout electronics was measured to be less than 0.2 MeV and 2 MeV for channels with high and low sensitivities respectively. These two factors determine the accuracy of the relative calibration.

The absolute calibration is usually provided by real physical processes. But in practice it is important to calibrate the calorimeter without particles.

The relation between energy deposition E_I in the gap of ionization chamber and the measured pulse height A is:

$$E_I = \frac{W}{F} \cdot \frac{A-b}{e \cdot a_g} \cdot \frac{a_g}{a_p},$$

where, W is the average energy required to produce an electron-ion pair, F is the recombination factor, e is an electron charge magnitude, b is the pedestal, a_g, a_p are the gain constants of the readout channel for the current pulses from the generator (I_g) and particle (I_p) respectively. The ratio a_g/a_p can be easy calculated if the shape of the current pulse I_p is known:

$$I_p(t) = \frac{Q_{tot}}{T_d} \cdot (1 - \frac{t}{T_d}) \cdot exp(-\frac{t}{T_\lambda}), \quad Q_{tot} = \frac{e \cdot E_I}{W},$$

where, T_d is the drift time and T_λ is the attachment lifetime for electrons of the ionization. The accuracy of the absolute calibration is determined by the measurement errors of the parameters W, F, T_d, T_λ.

There are few measurements of the W-value [10, 11, 12]. Really, the ratio W/F is measured in an experiment. We used the value

$$\frac{W}{F} = 18.3 \pm 0.3 \; eV/pair$$

measured for the charge collection at the highest electric field of 16 kV/cm [12] as the estimation of the W-value.

We measured the parameters T_d, T_λ, F. The method of the T_d and T_λ measurements was based on the analysis of the waveform of the signals from cosmic rays and β-radioactive isotop ^{90}Sr (will be published). At the applied electric field of 513 V/cm the parameters T_d, T_λ, F were found to be 9.0±0.2μs, 2.85±0.15μs, 0.78±0.02, respectively.

We compared the energy scale constant obtained from the electronics absolute calibration (S_g) with one obtained from the edges of Compton and bremsstrahlung spectra (S_γ). The ratio of the scale constants was found to be S_g/S_γ = 1.01±0.03., where the error is determined by the accuracy of absolute calibration.

3..2 Noise

There are three different sources of the noise: the electronic noise (N), the noise of radioactivity (R) and coherent noise (C).

The electronic noise measured in electrons can be parameterized as

$$N = N_0 + \alpha \cdot C_{det},$$

where, N_0 is the noise of unloaded preamplifier, α is a noise slope constant, C_{det} is a detector capacitance. The typical parameters N_0 and α for the preamplifiers based on $FET\ NJ1800D$ are shown in Table 2. The parameters were measured for different shaping times (τ) and filters.

Table 2. The noise of electronics

τ	RC-CR		2RC-CR		RC-2CR	
μs	$N_0, el.$	$\alpha, el./pF$	$N_0, el.$	$\alpha, el./pF$	$N_0, el.$	$\alpha, el./pF$
0.5	1000	3.10	902	2.47	1263	4.32
1.0	898	2.48	811	1.92	1092	3.39
2.0	828	1.67	748	1.11	968	2.50
3.0	772	1.37	695	0.94	881	1.90
4.0	747	1.21	673	0.87	877	1.65
5.0	707	1.04	656	0.76	850	1.33

The detector capacitance is the sum of the gap capacitance (C_d≈190 pF) and cross-talk capacitance (C_a≈40 pF between two adjacent cells) as it is shown in figure 6. For the typical value of the detector capacitance of 350 pF and τ=1μs the electronic noise is 2300 electrons.

The electronic noise has to be treated together with the LKr radioactivity. The natural krypton contains small admixture of the β–radioactive isotop ^{85}Kr with activity of ~300 $decays/sec$ in 1 cm^3 of LKr. The events of β–decay produce point-like ionization in the gap of the chamber. It results in the random consequence of rectangular shape current pulses in the input of the preamplifier and can be considered as an extra source of noise (pile-up noise) [9].

In figure 5 the measured noises $N+R$, N and R for applied high voltage of 1 kV and different τ are shown. The electronic noise was measured at switched off high voltage. Since the value of the R-noise depends on the shaping time as $\sim\sqrt{\tau}$ and the N-noise decreases with τ, there is the optimal shaping time $\tau_{opt}\approx 1\mu s$ (τ=1.05μs was in the experiment). In order to select the contribution of the R-noise we subtracted in quadrature the noise of electronics from the total noise $N+R$.

For the strip channels the noise of radioactivity is negligible because of the small detection volume. To reduce the noise of electronics the shaping time of 5.2μs for the strip channels was selected. The electronic noise was measured to be 0.15 MeV. The pick-up noise was estimated to be 0.3 MeV and 0.1 MeV for the first and two next strip layers respectively.

The presence of the coherent noise is evinced in the procedure of summing the amplitudes of separate channels which are used to reconstruct the total amplitude. Actually the variance of the total amplitude σ_t is not equal to the sum

$$\sigma_\Sigma^2 = \sum_{i=1}^{n} \sigma_i^2,$$

where, σ_i is the noise of channel i, n is the number of channels. The σ_t depends on the level of pick-up noise and the configuration of cells taken in the sum. The average coherent noise can be estimated as

$$\sigma_c^2 = \frac{1}{n-1}\cdot\left(\frac{\sigma_t^2}{n} - \frac{\sigma_\Sigma^2}{n}\right).$$

The coherent noise has two components: correlated (pick-up) noise ($\sigma_c^2 > 0$) and anticorrelated noise ($\sigma_c^2 < 0$).

The anticorrelated noise is described by presence of the cross-talk capacitance between two adjacent cells. The cross-talk capacitance doesn't give contribution to the total electronic noise of such two channels.

For example we simulated the configuration of 5 cells (like in fig. 6). The capacitors which simulated C_d and C_a had capacitances of 470 pF each. The

results of the noise measurement for different configurations of the preamplifiers are shown in Table 3, where, m_t is the total number of capacitors in the configuration and m_e is the number of capacitors which give contribution to σ_t. The total noise of $(1+2+3+4+5)$ configuration doesn't depend on the cross-talk capacitance.

Table 3. The noise of electronics for different configurations of the channels and the fixed value of the cross-talk and detector capacitances of 470 pF.

configuration	n	m_t	m_e	$\sqrt{\sigma_\Sigma^2/n}$, $el.*10^{-3}$	$\sqrt{\sigma_t^2/n}$, $el.*10^{-3}$
1	1	5	5		8.9
2,3,4 or 5	1	2	2		4.3
2+3+4+5	4	8	8	4.4	4.3
1+2+3+4+5	5	13	5	5.6	2.7

To estimate the pick-up noise we used the configurations of channels which haven't anticorrelated components of the noise. We turned the special attention to the suppression of the pick-up noise in the tower channels. Its residual level was achieved to be less than 0.2 MeV (Table 4).

Table 4. The pick-up noise for different τ. The measurement errors are 10%.

τ, [μs]	0.50	1.05	2.20	3.30
σ_c, [electrons]	270	830	970	800
σ_c, [MeV]	0.12	0.21	0.15	0.13

3..3 Cross-talks and long-term stability

The cross-talks between the electronic channels were measured using the calibration generator. There was no the cross-talk signal exceeded 0.2%.

The sources of the cross-talk in the electrode system are the cross-talk capacitances C_a. Since the total input capacitance C_{in} of the preamplifier is large, the fraction of the cross-talk charge is quite small

$$F_c = \frac{4\cdot C_a}{C_d + 4C_a + C_{in}}, \qquad C_{in} = \left(\frac{1}{C_l} + \frac{1}{C_h}\right)^{-1},$$

where, C_h is the capacitance of a high voltage capacitor (12 nF), C_I is the input capacitance of the preamplifier ($50 \div 60$ nF for $\tau = 1\mu s$). We measured the cross-talk signal using the cosmic particles and found it equal to $1.1 \pm 0.1\%$, that is in a good agreement with the expected cross-talk: 1.2%.

The long-term stability was measured using the calibration runs which were written down during the time of experiment of 60 days. To estimate the stability we calculated the relative deviations of the gain constants from the average one for each channel. The distributions on the relative deviation for all tower channels are shown in figure 7. The variances of the gain constants are 0.4% and 1.5% for the channels with high and low sensitivities respectively.

4. The tagged photon beam setup

The experiment was performed at the facility $ROKK-1M$ [13] of the $VEPP-4M$ collider. It includes the Nd:YAG laser, the optic system to transfer the laser photons to the electron beam and the detector KEDR Tagging System [14]. The layout of the $ROKK-1M$ and the $VEPP-4M$ experimental area is shown in figure 8.

High energy photons are produced in the backward Compton scattering of the laser photons on the colliding electron beam. The maximum energy of the scattered photons is:

$$E_{max} = \frac{4\omega\gamma^2}{1 + 4\omega\gamma/mc^2},$$

where ω is the energy of a laser photon (2.34 eV), γ is the beam relativistic factor and m is an electron mass.

The scattered photons move in the direction of the electron beam and are detected by the calorimeter. There are the collimator and veto scintillation counters in front of the calorimeter.

The scattered elcctrons (SE) are detected by means of the tagging system (TS). The tagging system includes two bending magnets (M1,M2), the doublet of mini–β quadrupoles (Q1,Q2) and four drift tubes hodoscopes (TS1-TS4) for the measurement of the SE transverse coordinate. The bending magnets deflect from the beam those electrons which have lost part of their initial energy. The magnets and quadrupoles form a focusing spectrometer for the scattered electrons energy measurement. Due to the focusing properties of the quadrupoles the transverse coordinate of the scattered electron is independent on it emission angle. So only the transverse coordinate

is sufficient to measure in order to determine the energy of the scattered electron.

For tagging of the high energy photons we used the $TS4$ hodoscope which detects the scattered electrons if their energy is between 3% and 15% of the beam energy.

The energy resolution of the tagging system is determined mainly by the beam angle spread and spatial resolution of the TS. The typical energy resolution of the TS for photons is about 1.3%.

The beam energy was varied during the experiment between 1.5 GeV and 4.5 GeV, thus the tagged photon energy region was $40 \div 625$ MeV. Besides that we used the independent method of the energy resolution measurement. It was based on the analysis of the edges of the Compton spectra. The edges of the bremsstrahlung spectra were used for the energy resolution measurement in the high energy region up to 4500 MeV.

5. Energy measurements

5..1 The expected energy resolution

Showers produced in LKr were simulated by Monte-Carlo method for the real structure of the calorimeter. The energy resolution of the calorimeter is determined by the following factors:

- Geometric (induction) effect
- Variation of the gap
- Electronic noise
- Radioactivity of LKr
- Pick-up noise
- Sampling fluctuations in the dead material
- Energy leakage fluctuations
- Algorithm of the energy reconstruction.
- Calibration inaccuracy, instability of electronics

The geometric effect (G) arises from the dependence of the collected charge on the ionization distribution inside the gap. The contribution of this effect is proportional to the fraction of the collected charge τ/T_d. In our experiment ($\tau/T_d \approx 0.1$) the contribution of this effect is

$$(\frac{\sigma_E}{E})_G = \frac{1.2\%}{\sqrt{E(GeV)}}.$$

The contribution of the gap size variation (V) depends on the ratio σ_d/d, where d is a gap width, and σ_d – its rms variation. The contribution of this effect was found to be

$$(\frac{\sigma_E}{E})_V = \frac{\sigma_d}{d} \cdot \frac{0.12\%}{\sqrt{E(GeV)}}.$$

We estimate the mechanical accuracy of the gap size in the calorimeter to be better than 1 mm.

The noise ($N+R+C$) was taken in to account by mixing of the measured noise into each tower amplitude calculated in the Monte Carlo simulation.

For high energy photons ($E_\gamma > 1\ GeV$) 3×3×3 block (27 cells) is used for the energy reconstruction and the energy leakage is determined by the longitudinal leakage. The Monte-Carlo data for the sum of longitudinal leakage (L) and sampling fluctuations (S) are well fitted by the simple formula:

$$(\frac{\sigma_E}{E})_{L+S} = 0.8\% + \frac{0.3\%}{\sqrt{E(GeV)}}.$$

For low energy photons ($E_\gamma < 1\ GeV$) there should be compromise between the leakage and noise contributions and only some part of the towers from 3×3×3 block is sufficient to use in the analysis.

The expected energy resolution as a function of photon energy is shown in figure 9. All mentioned above effects are taken into account. The results of two various algorithms are presented in the plot; the first one — all 27 amplitudes are used in the analysis, another one — only the amplitudes which exceed 2.2 MeV are used.

The experimental results were obtained using the second algorithm.

5..2 The experimental energy resolution

Data were collected during March–May, 1994 at the electron beam energy of 1.5, 1.8, 2.0, 2.4, 3.0, 3.5, 4.0, and 4.5 GeV. For the measurement of

the energy resolution we used, as it was mentioned above, two independent methods.

In the first one the data from LKr calorimeter were written down together with the information from the tagging system. The photon energy measured in LKr versus the energy measured by TS is plotted in figure 10 for the electron beam energy of 4.5 GeV. The similar plots were built for the runs at all other beam energies. The monochromatic samples of photons were selected using the TS information.

The energy resolution is obtained from histograms on the energy deposition in LKr collected for each sample. The typical histogram is shown in figure 11. The fit is made using a logarithmic normal distribution:

$$\frac{dp}{dx} = \frac{1}{\sqrt{2\pi}} \cdot exp\left\{-\frac{1}{2} \cdot \left[\frac{ln^2(1+ax)}{a^2} + a^2\right]\right\},$$

$$x = \frac{f(E-E_p)}{\sigma}, \quad \sigma = \frac{FWHM}{2.36}, \quad f = \frac{sh(a\sqrt{ln4})}{a\sqrt{ln4}},$$

where, E is the energy parameter, E_p is the peak energy, a is conventional asymmetry. The free parameters of the fit are E_p, σ, a. The energy resolution of the calorimeter (σ_E/E) is determined by the fit after subtracting in quadrature the contribution of the TS resolution.

Another independent method of the energy resolution measurements is based on the analysis of the edges of Compton spectra. The natural width of the spectrum edge is determined by the radiative corrections. In our case, when the c.m.s photon energy is much less than the electron mass, their contribution is negligible. The typical Compton spectrum obtained in the experiment is shown in figure 12. Such histograms were fitted by the function defined as a convolution of the theoretical Compton spectrum with a logarithmic normal shape of the calorimeter response.

The results obtained by these two methods in the energy region below 629 MeV are shown in figure 13 together with the data of Monte Carlo simulation. The experimental results are in a good agreement to each other as well as to the Monte Carlo simulation.

At high energies the analysis of the edges of the single bremsstrahlung spectra was used for the energy resolution measurement. The spectra was described by the QED formula for the single bremsstrahlung process with an arbitrary screening [15, 16]. The results are in a reasonable agreement with the Monte Carlo simulation. The data obtained in whole energy region between 40 and 4500 MeV are shown in figure 14 in a logarithmic scale. All the experimental data are well fitted by the function:

$$\frac{\sigma_E}{E}\,(\%) = \sqrt{\left(\frac{a}{E(GeV)}\right)^2 + \left(\frac{b}{\sqrt{E(GeV)}}\right)^2 + c^2}$$

with $a = 0.3$, $b = 1.6$, $c = 1.6$.

5..3 The temperature stability of the calorimeter response

The density (ρ) of the liquid, the drift velocity (V_d) and absorption length (λ) of free electrons in the liquid have dependence on the temperature. It results to the instability of the calorimeter response if the liquid's temperature is varied with time.

The variation of ρ on the temperature for LKr is $-0.4\%/K$. It gives contribution to the measured amplitude for minimum ionization particles and doesn't give contribution for showers.

Since the fraction of the collected charge in our experiment was small, the calorimeter response is proportional to the drift velocity. We measured the variation of V_d on temperature for LKr (fig. 15) and have found it to be $-0.8\%/K$. This value was almost independent on the purity of the gas.

We measured the temperature dependence of the calorimeter response during two runs. In the first run we worked with cosmic particles. The particular feature of this run was small lifetime of electrons $T_\lambda = 0.3\mu s$. The measured variation of the amplitude A_{mip} on T is shown in figure 16. The relative variation of the calorimeter response is

$$\frac{1}{A_{mip}} \cdot \frac{dA_{mip}}{dT} = -1.3 \pm 0.2\ \%/K,$$

that is in a good agreement with the expectation: $-1.2\%/K$. In the second run we worked with another sample of gas ($T_\lambda = 3\mu s$) and measured the same value for showers (fig. 17):

$$\frac{1}{A_\gamma} \cdot \frac{dA_\gamma}{dT} = -0.40 \pm 0.05\ \%/K.$$

It is less then the expected value: $-0.8\%/K$.

6. Coordinate measurements

6..1 The coordinate reconstruction

Compare to the crystal calorimeters where the space resolution is limited by the fluctuations of the shower center of gravity, in the LKr calorimeter a considerably better space resolution can be obtained. Thanks to the strip structure in the first section of the calorimeter the position of the beginning of the shower is measured.

At low energy ($E_\gamma < 300\ MeV$) the space resolution is determined mainly by multiple scattering, at high energy it depends on the readout method. For the anode readout mode the space resolution is determined by a strip width ($\sigma \approx 3\ mm$). For the cathode readout mode the resolution is much better ($< 1\ mm$) [4, 2].

In the cathode readout mode few strips are sensitive to an ionization in the drift gap and the center of gravity methode can be used for the coordinate reconstruction:

$$Y_n = \frac{\overline{a \cdot x}}{\overline{a}}, \qquad \overline{a \cdot x} = \frac{1}{n}\sum_{i=1}^{n} a_i x_i, \qquad \overline{a} = \frac{1}{n}\sum_{i=1}^{n} a_i,$$

where a_i is the charge induced on the strip i, x_i is the strip coordinate, n — number of the strips. The width of the charge distribution over the strips is equal approximately to the gap size, therefore two or three strips with maximum amplitudes are sufficient to use in the analysis. The center of gravity coordinate Y_n is a nonlinear and discontinuous function of the real coordinate X. The functions $Y_2(X)$ and $Y_3(X)$ have jumps in the middle of a strip and between strips respectively (fig. 18). To make the function smooth the "generalized" center of gravity coordinate can be used:

$$Y_g = Y_2 \cdot \frac{a_2 - a_3}{a_1 - a_3} + Y_3 \cdot \frac{a_1 - a_2}{a_1 - a_3}, \qquad a_1 > a_2 > a_3.$$

6..2 The experimental results

For the experimental study of the space resolution, several runs with the collimated photon beam were performed. In these runs the lead collimator with a thickness of 80 mm and 1 mm split parallel to the strips in the calorimeter was placed in front of the cryostat. Between the collimator and the calorimeter the veto counter was installed for the suppression of the background showers. The collimator moved across the strip direction and its position was measured with an accuracy of 0.1 mm.

During the runs the coordinates of the beam position were measured in 11 points of the strip structure with a step of 1 *mm*. Depending on the conversion point there were 1÷3 coordinate measurements for a single photon. Therefore, three data samples $\{X_\gamma^1, X_\gamma^2, X_\gamma^3\}$ were available in each run, where X_γ^1 is the coordinate measured in a layer where the first interaction of the photon take place, X_γ^2, X_γ^3 are the coordinates in the next layers.

To determine the functions $Y_g^i(X)$ $(i = 1, 2, 3)$ we measured the average center of gravity coordinates $\overline{Y_g^i}$ in each run (fig. 18). The measured dependences $\overline{Y_g^i}$ on X were fitted by smooth functions. These functions were used to determine the photon coordinates X_γ^i from the center of gravity coordinates.

In figure 19 the distributions on the Y_g and X_γ coordinates are shown. The variation of the distribution on X_γ gives the space resolution of the calorimeter, if the *rms* width of the collimator split is subtracted. The resolution depends slightly on the coordinate across the strip (fig. 20). The average space resolution for different energies of the photons is shown in figure 21. The results are in a good agreement with the Monte Carlo simulation.

Since the electronic noise is rather small (see section 3.2) the best space resolution is obtained in the layer where the first conversion of a photon into e^+e^- pair take place. The resolution in the next layers is affected by multiple scattering.

7. Conclusions

The described LKr calorimeter combines the energy resolution proper to the crystal calorimeters with excellent space resolution for photons in a wide energy region.

The energy resolution was measured in the experiment at the tagged photon beam in the energy range between 40 and 625 MeV. The energy resolution 6% at 0.1 GeV and 2.2% at 1 GeV have been obtained. The results are in a good agreement with the expected energy resolution.

The spatial resolution much better then one for crystal calorimeters have been obtained: 1.2 *mm* at 0.2 GeV and 0.8 *mm* at 1.0 GeV.

The temperature stability of the calorimeter response have been measured. It is different for particles with minimum ionization and showers: $-1.3\%/K$ and $-0.4\%/K$ respectively.

We tested the final version of the readout electronics for LKr calorimeter of $KEDR$ detector. The charge sensitive preamplifiers based on FET $NJ1800D$ provide the measurement of the collected charge for the tower and

strip channels with the low level of noise. The readout electronics has a good linearity and long-term stability.

8. Acknowledgments

The authors would like to express their gratitude to professor A.N.Skrinsky and professor V.A.Sidorov for a support and for $VEPP$–$4M$ staff whose efforts made this work possible and to V.M.Katkov and V.M.Strakhovenko for the assistance in the analysis of the bremsstrahlung spectra. We wish to thank V.A.Rodyakin and R.G.Snopkov for help in the prototype assembling.

This work was supported by Russian Found of Fundamental Research (grant number: 94-02-03995) and partially supported by International Science Foundation (grant number: JDA100).

References

[1] V.M.Aulchenko et al. Proc. of the 24 Int. Conf. on High Energy Physics, Munich, 1988 (contrib. paper) V.V.Anashin et al. Proc. of the Int. Symp. on Position Detect. in High Energy Physics, Dubna, 1988, p.58

[2] V.M.Aulchenko et al., Proc. Int.Conf. on Calorimetry at High Energy Physics, FNAL, 1990. Editor F.Anderson, World Scientific, p.223.

[3] P.Cantoni et al., Nucl.Instr.and Meth. A315 (1992) 491

[4] V.M.Aulchenko et al. Nucl.Instr.and Meth. A289 (1990) 468

[5] V.M.Aulchenko et al. Nucl.Instr.and Meth. A316 (1992) 8

[6] V.M.Aulchenko et al. Nucl.Instr.and Meth. A327 (1993) 194

[7] G.D. Barr et al., Performance of an Electromagnetic Liquid Krypton Calorimeter based on a Ribbon Electrode Tower Structure. CERN-PPE/95-64, 21 April 1995.

[8] V.M.Aulchenko et al., Preprint INP 88-29, Novosibirsk (1988).

[9] V.S.Panin, S.V.Peleganchuk, Preprint BINP 95-26, Novosibirsk (1995).

[10] S.Huang and G.R.Freeman, Can. J. Chem., 55, 1838(1977).

[11] T.Takahashi et al., J. Phys. C:Solid State Phys., 7, 230(1974).

[12] E.Aprile et al., Phys.Rev. A, V48, N2, 1993, p.1313.

[13] G.Ya.Kezerashvili et al., Proceed. of XXII International Conference on the Accelerators of High Energy Charged Particles, Dubna (1992), V.1, pp.416-418.

[14] A.E.Bondar et al., Proceed. of XXII International Conference on the Accelerators of High Energy Charged Particles, Dubna (1992), V.1, p.309.

[15] V.N.Baier, V.M.Katkov, V.S.Fadin, Izluchenie Relativistskich Electronov, p.321., Moscow, Atomizdat (1973) (in russian)

[16] V.M.Strakhovenko, private communication

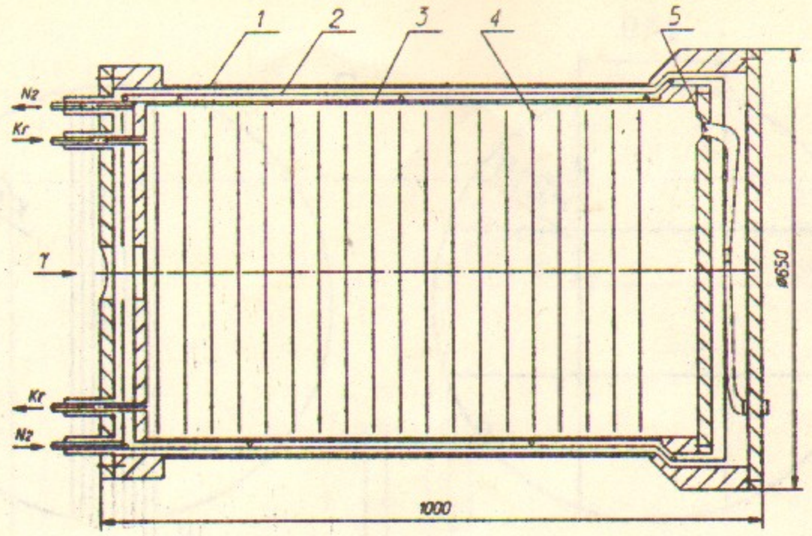

Figure 1. Layout of the prototype (a): 1 – external vessel, 2 – copper shield, 3 – internal vessel, 4 – electrode, 5 – output cable. Electrode system of the prototype (b): 1 – electrodes with strips, 2 – electrodes with pads, L1 – L3 — towers.

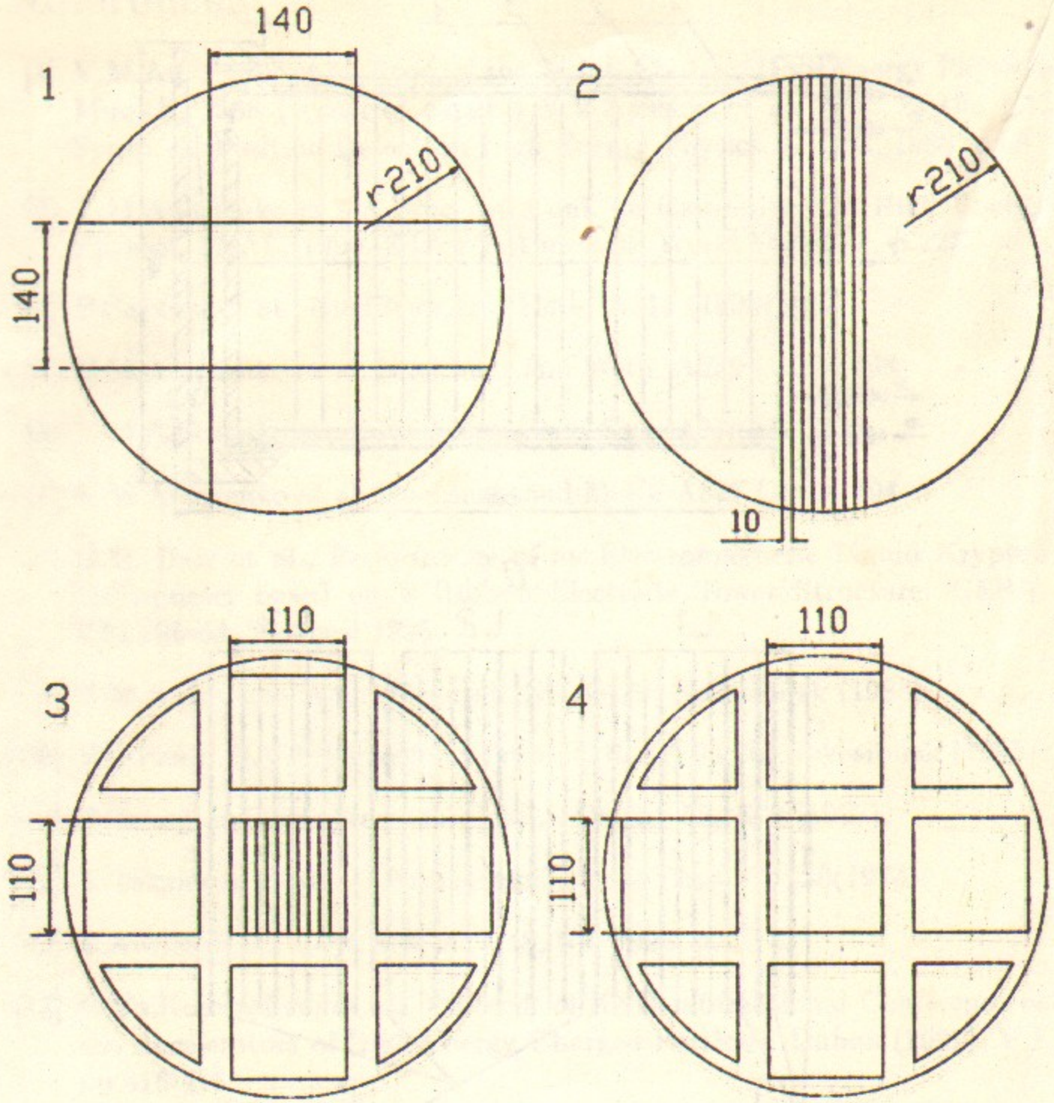

Figure 2. High voltage and "grounded" electrodes. 1 – high voltage electrode, 2 – electrode with strips, 3 – electrode with strips and pads, 4 – electrode with pads.

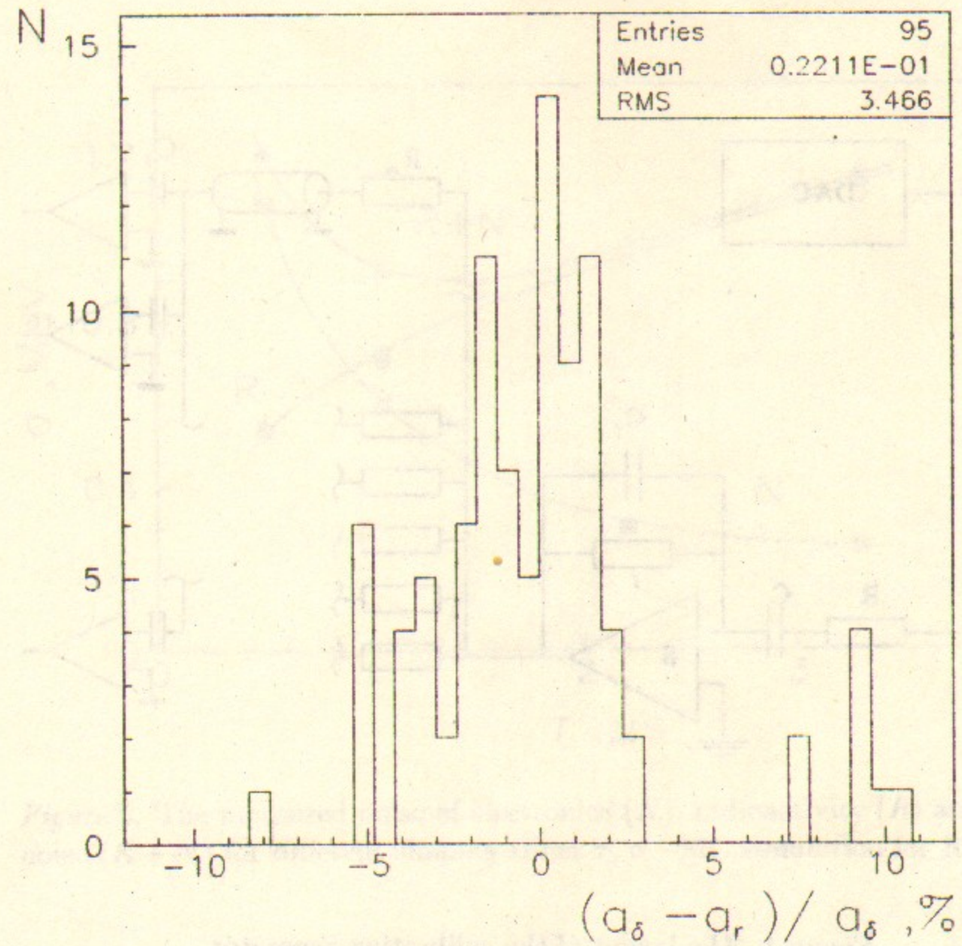

Figure 3. The difference of the gain constants obtained with the δ (a_δ) and "real" (a_r) shape calibration signals.

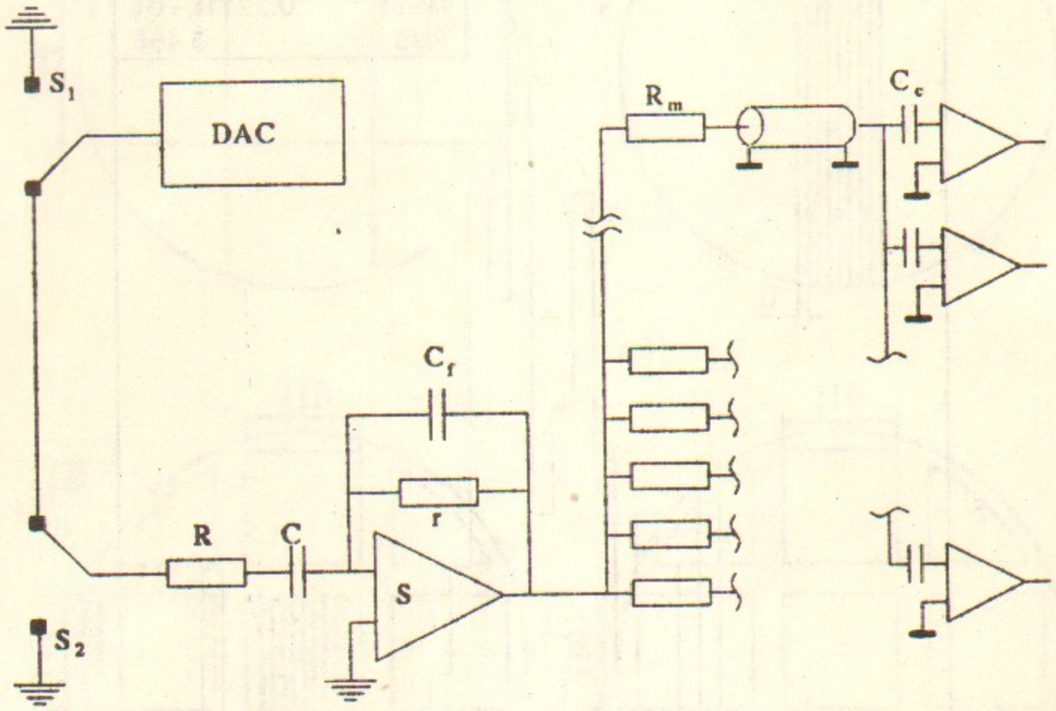

Figure 4. The layout of the calibration generator.

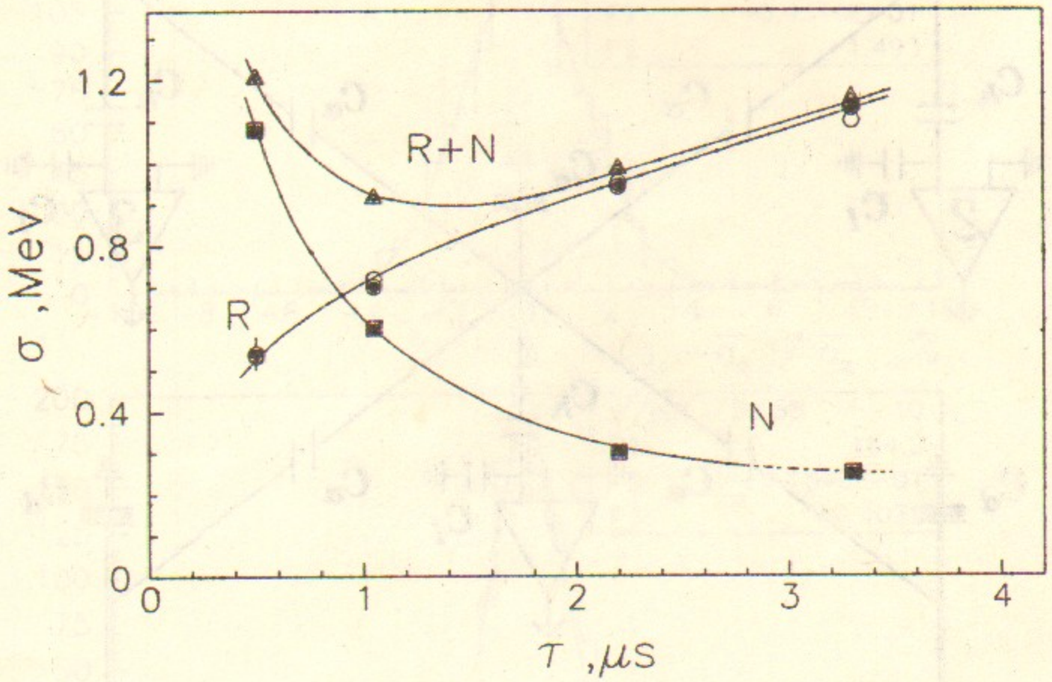

Figure 5. The measured noise of electronics (N), radioactivity (R) and total noise ($R+N$) for different shaping times τ, ∘ – MC simulation for R.

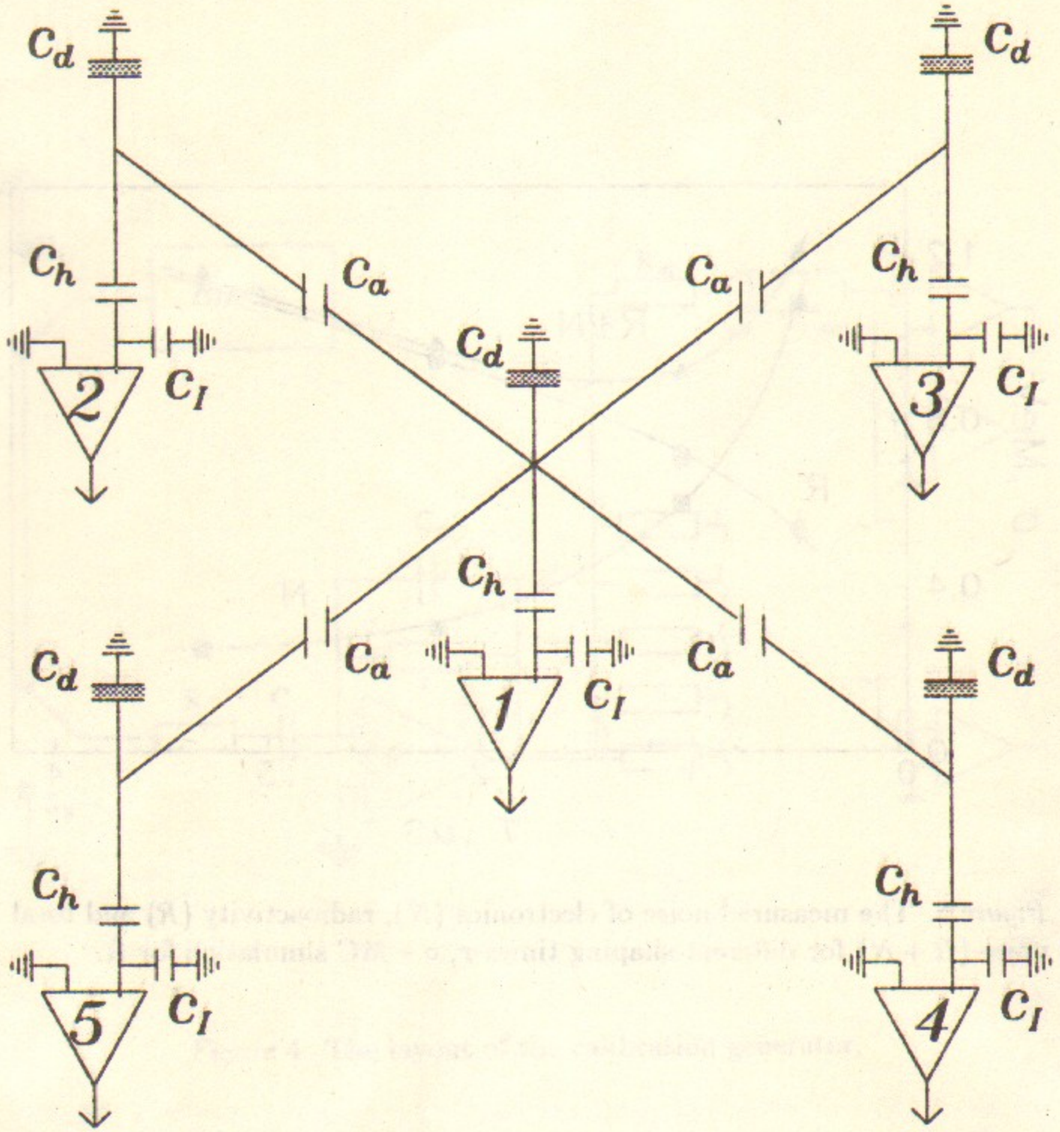

Figure 6. The readout configuration of the preamplifiers.

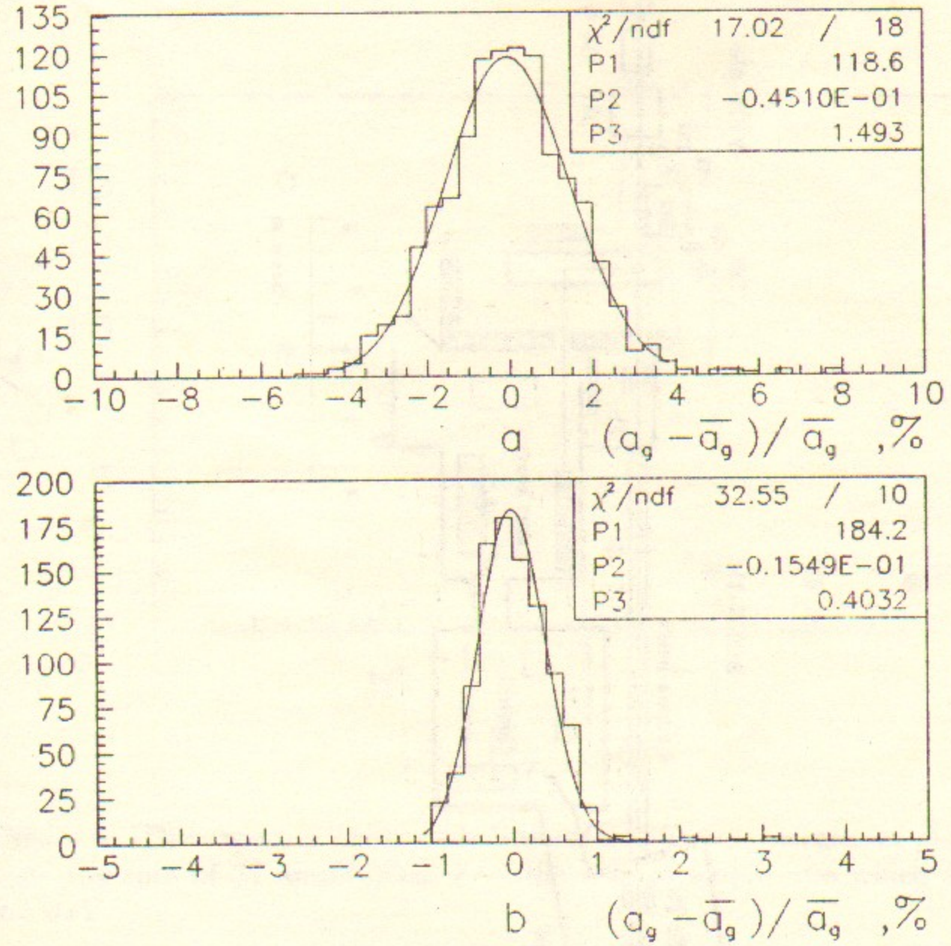

Figure 7. The distributions on the relative deviation of the gain constants for all tower channels: a – the channels with low sensitivity, b – the channels with high sensitivity.

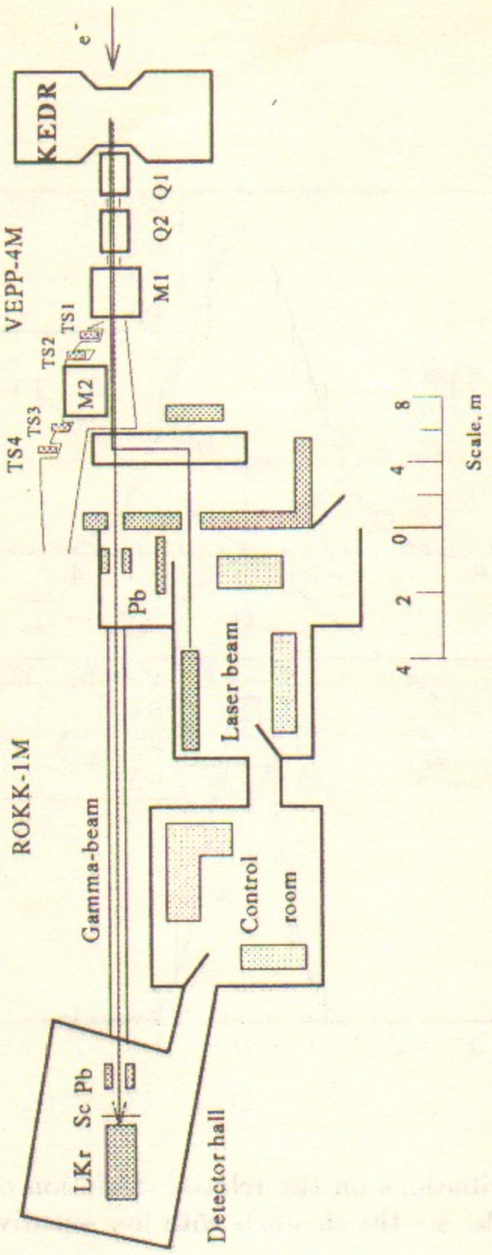

Figure 8. The layout of the $ROKK-1M$ and $VEPP-4M$ experimental area.

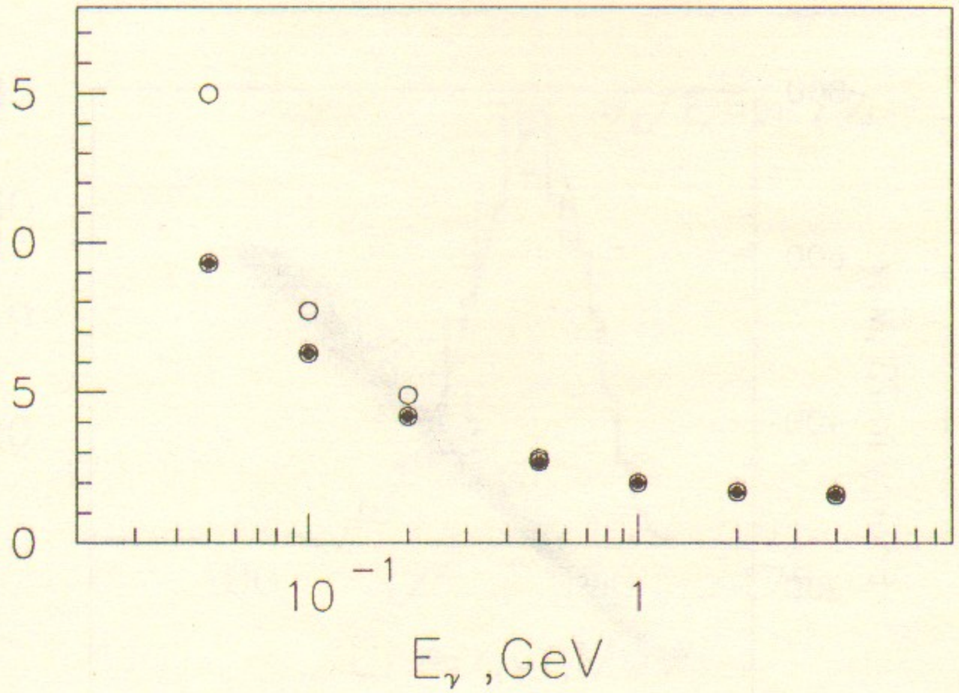

Figure 9. The expected energy resolution for different energies of photons: ∘ — the sum of 27 amplitudes, • — the sum of amplitudes which exceed $2.2MeV$.

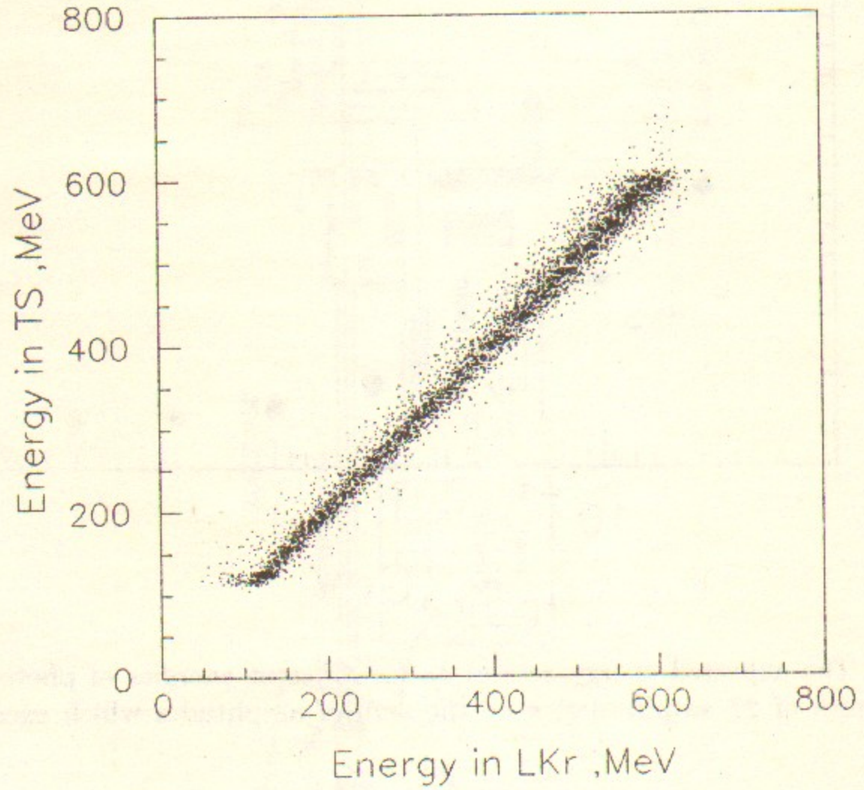

Figure 10. Photon energy measured in TS versus one measured in LKr.

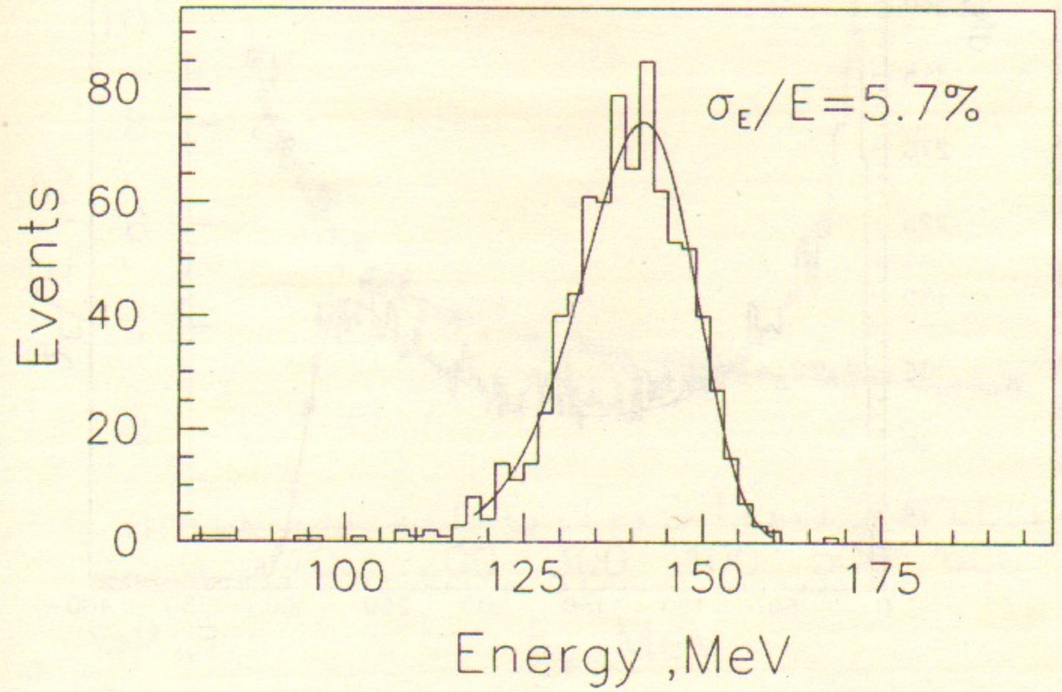

Figure 11. The measured energy deposition in the calorimeter for the monochromatic sample of photons. The fit is a logarithmic normal distribution.

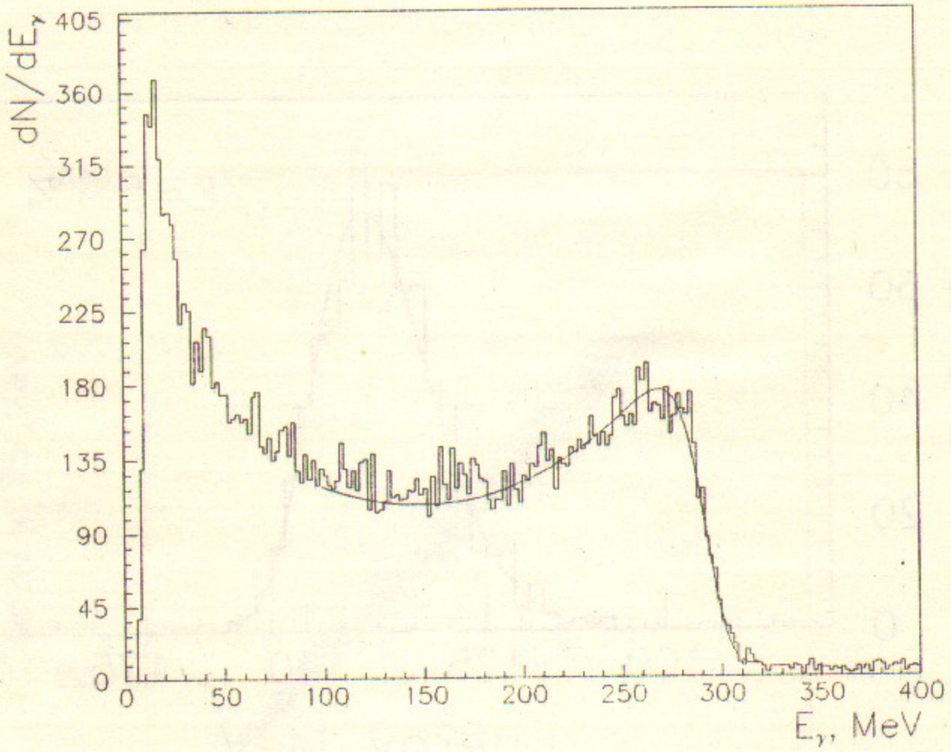

Figure 12. The typical Compton spectrum measured by the calorimeter (beam energy 3 GeV). Histogram is the experimental data, solid curve is the Compton spectrum convoluted with a logarithmic normal distribution. The high energy tail is described by the accidental coincidence of two photons.

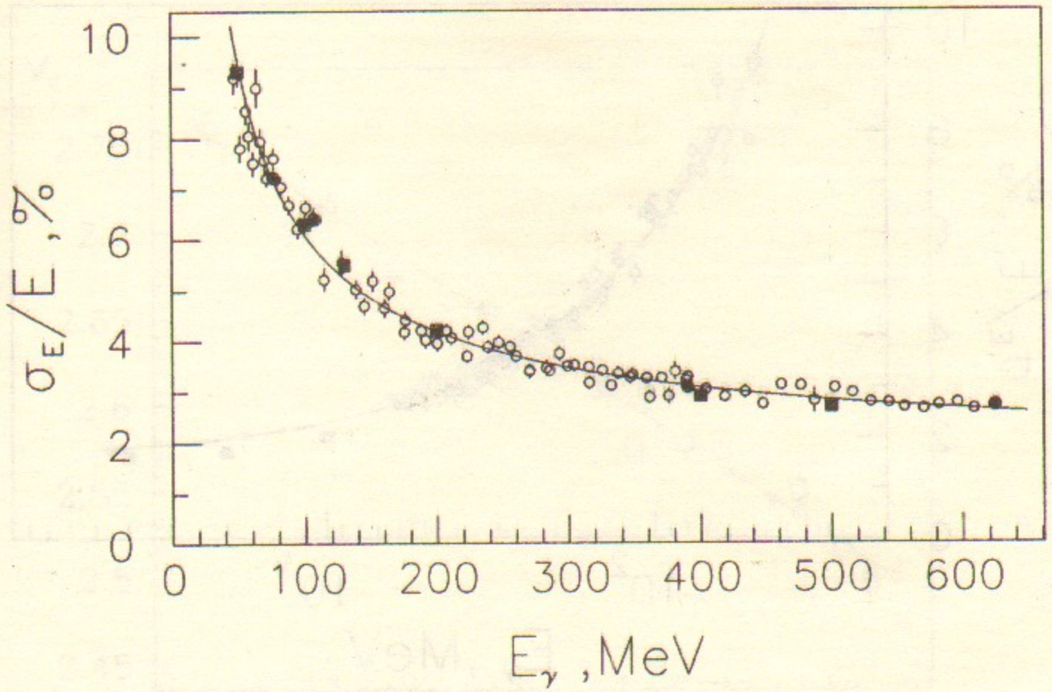

Figure 13. Energy resolution below 625 MeV: ∘ – the resolution obtained with the tagged photons, • – the resolution obtained by the fit of the Compton spectra, ■ – MC. — – the fit (see the text).

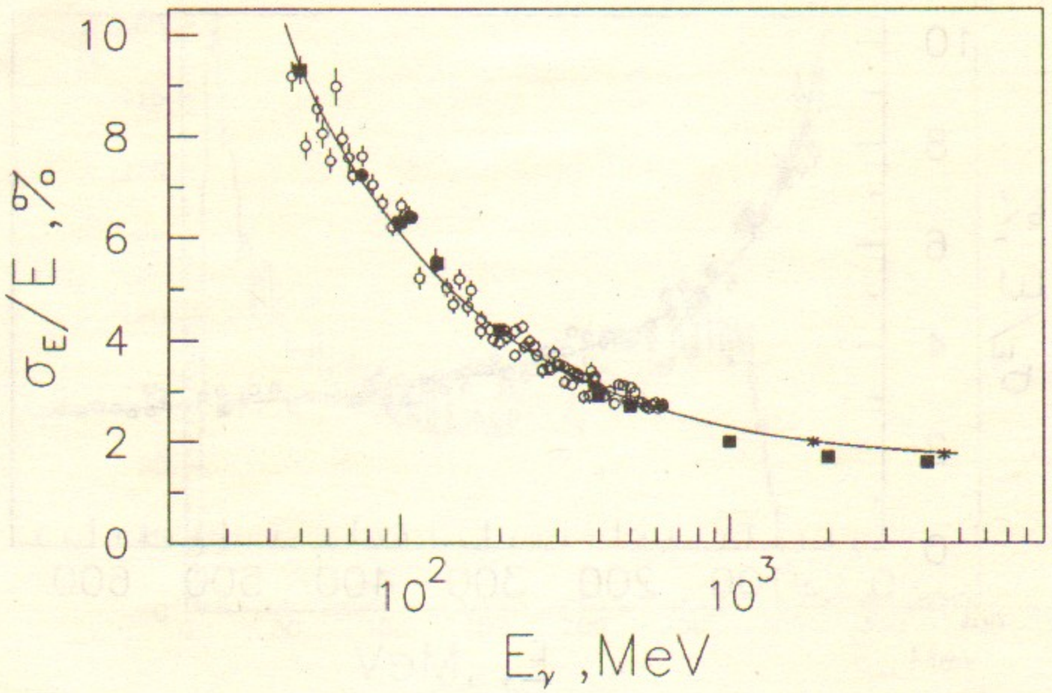

Figure 14. Energy resolution in the whole energy region: • – the resolution obtained by the fit of the Compton spectra, ∗ – the resolution obtained by the fit of the bremsstrahlung spectra, ■ – MC. — – fit.

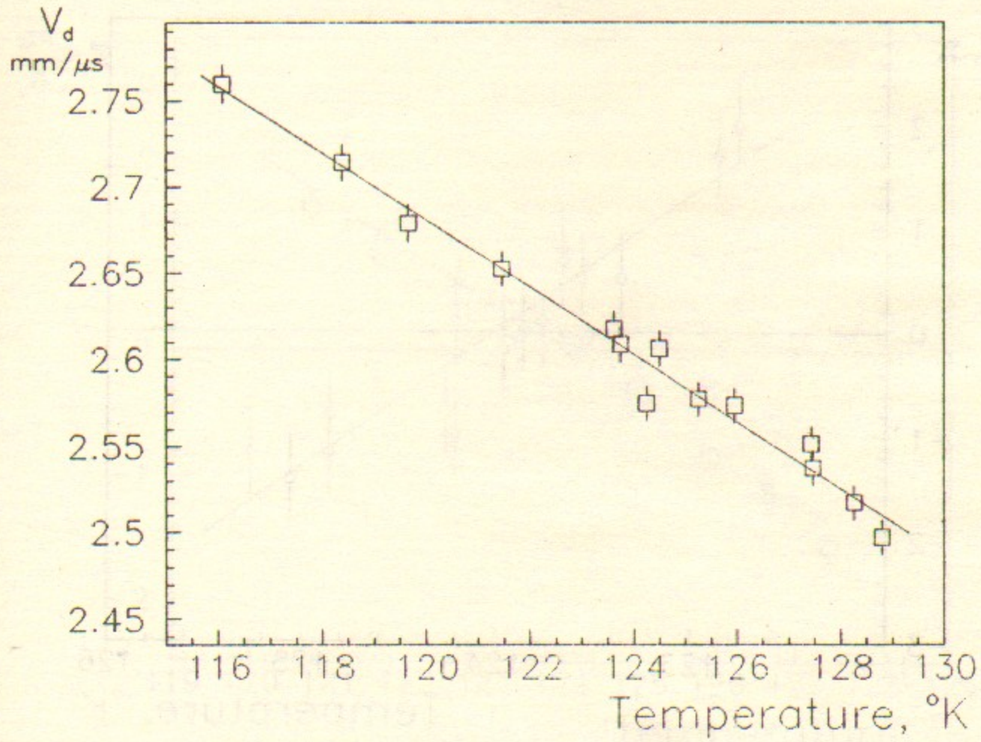

***Figure* 15. The measured dependance of the drift velocity on temperature.**

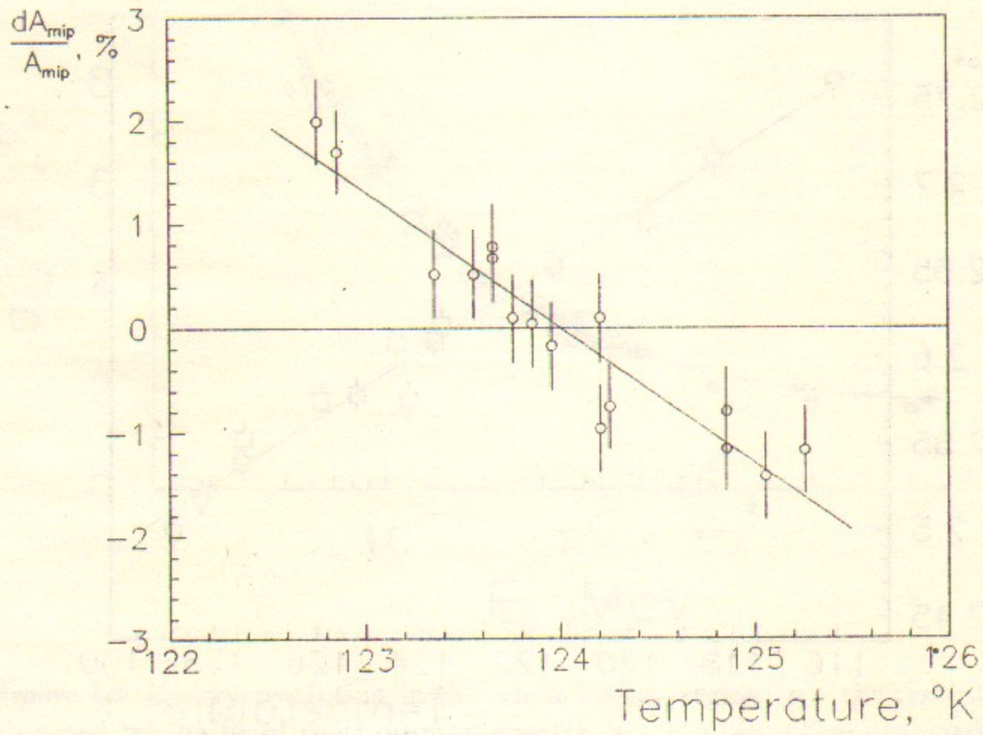

Figure 16. The measured dependance of the amplitude A_{mip} on T.

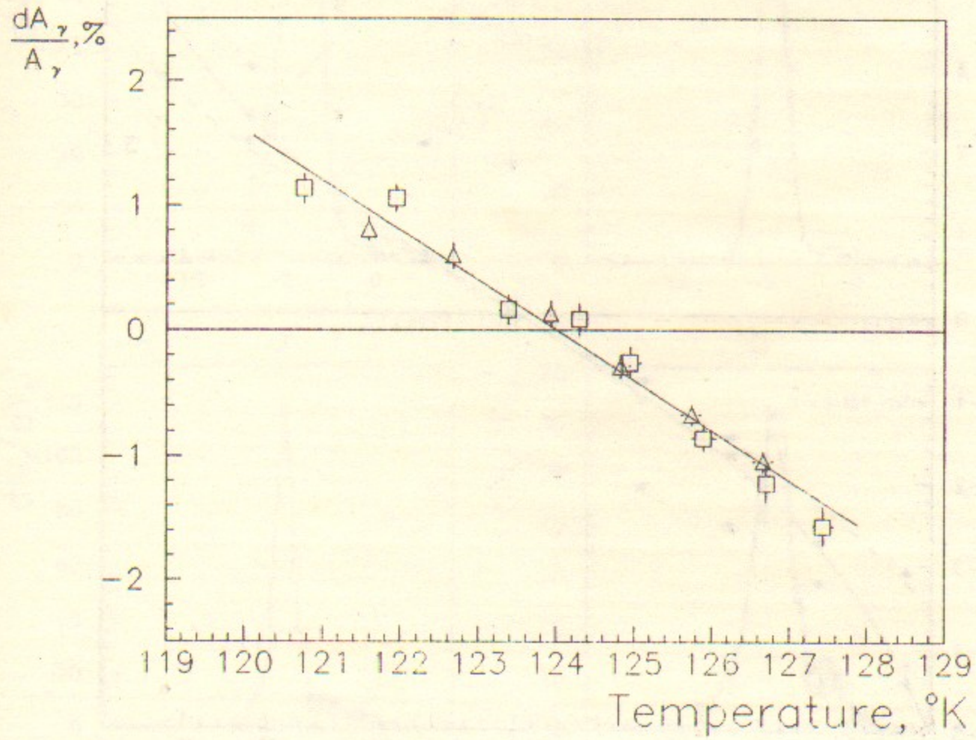

Figure 17. The measured dependance of the amplitude A_γ on T.

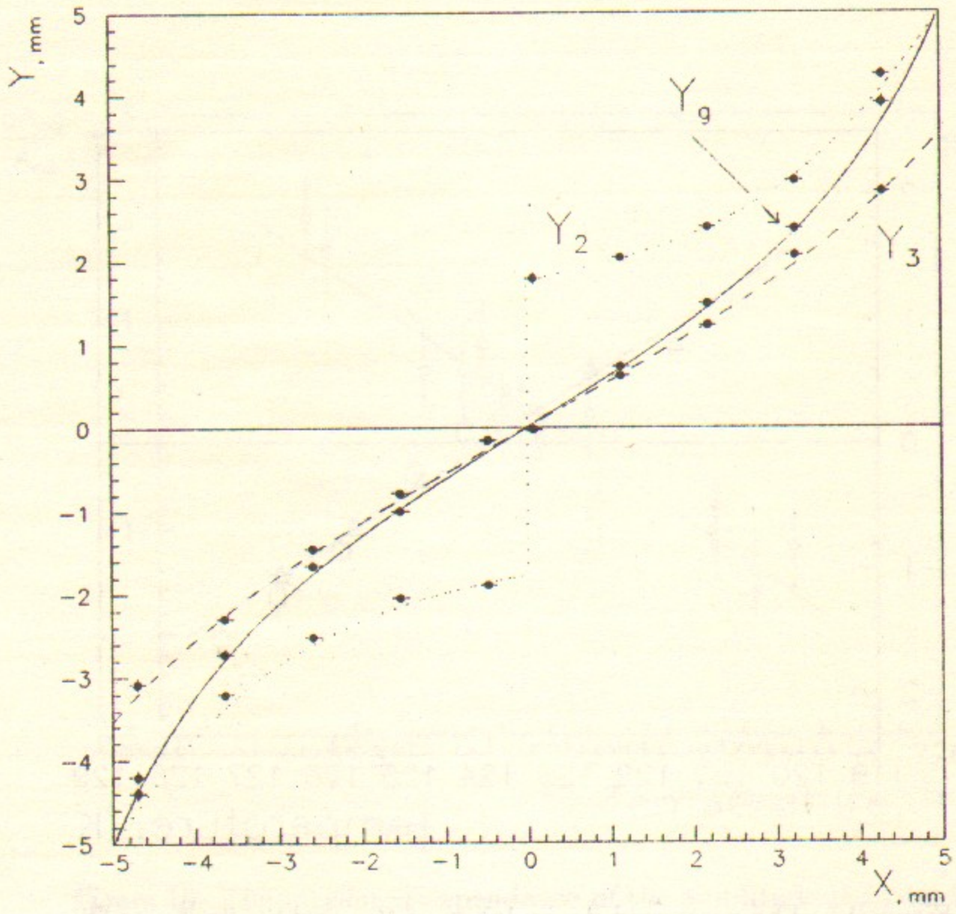

Figure 18. Center of gravity coordinate as a function of the photon coordinate. • – experiment, lines – fit.

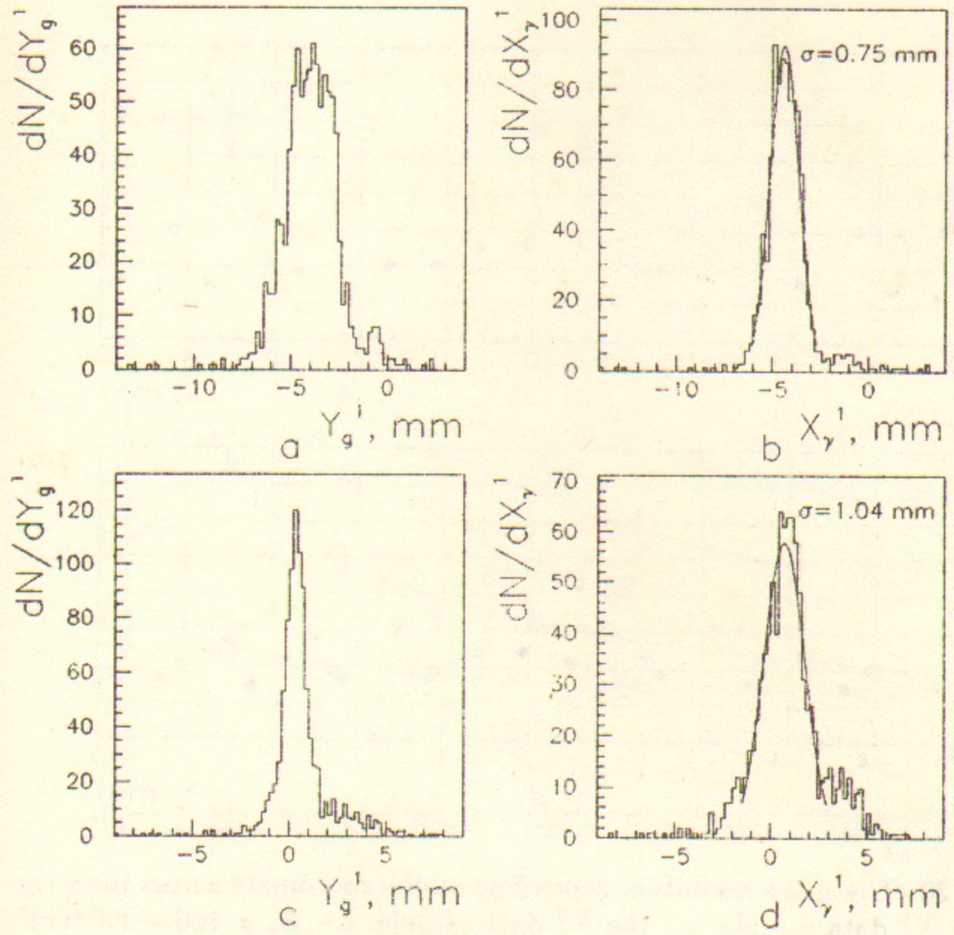

Figure 19. The distributions on the Y_g and X_γ coordinates: a-b — in the middle of strip, c-d — between strips.

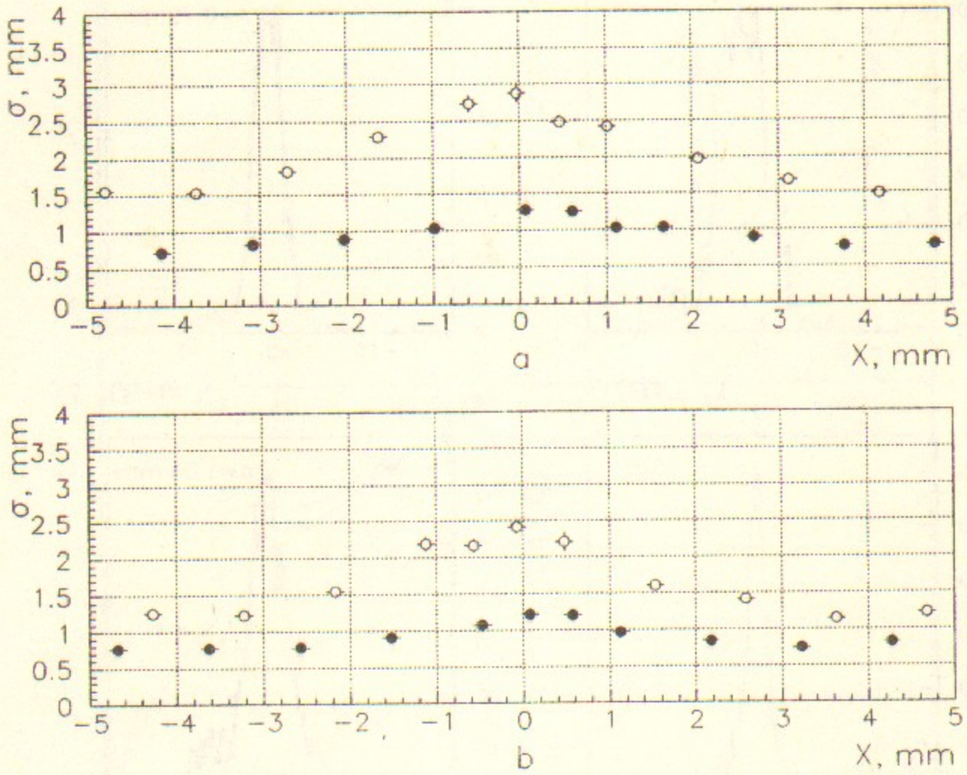

Figure 20. The space resolution depending on the coordinate across the strip: • – the X_γ^1 data sample, ∘ – the X_γ^2 data sample. a – $E_\gamma = 100 - 300 MeV$, b – $E_\gamma = 800 - 1200 MeV$.

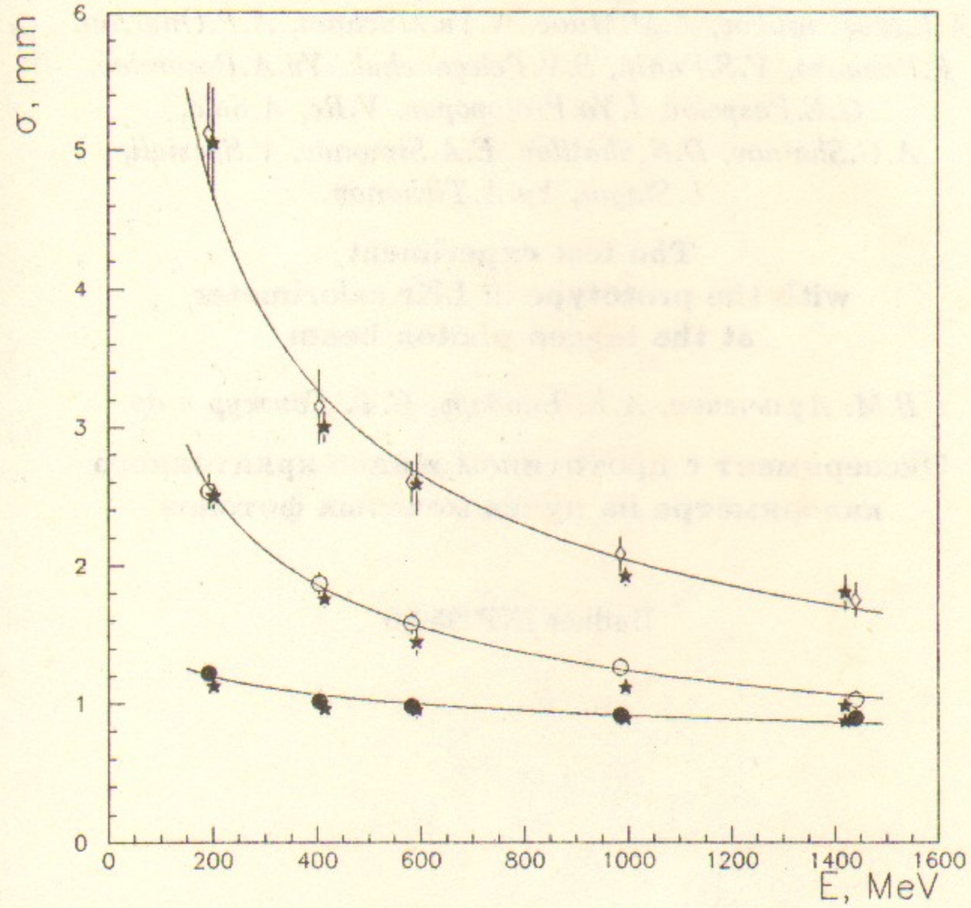

Figure 21. The space resolution depending on the photon energy: • – the X_γ^1 data sample, ∘ – the X_γ^2 data sample, ◇ – the X_γ^3 data sample, — – fit, ⋆ – MC simulation.

V.M.Aulchenko, A.E.Bondar, P.Cantoni, P.L.Frabetti,
S.F.Ganzhur, G.Ya.Kezerashvili, S.G.Klimenko, F.Lanni,
L.A.Leontiev, B.Maggi, V.M.Malyshev, P.F.Manfredi,
A.L.Maslennikov, A.M.Milov, N.Yu.Muchnoi, A.P.Onuchin,
F.Palombo, V.S.Panin, S.V.Peleganchuk, Yu.A.Pogorelov,
G.E.Pospelov, I.Ya.Protopopov, V.Re, A.Sala,
A.G.Shamov, D.N.Shatilov, E.A.Simonov, V.Speziali,
L.Stagni, Yu.A.Tikhonov

The test experiment
with the prototype of LKr calorimeter
at the tagged photon beam

В.М. Аульченко, А.Е. Бондарь, С.Ф. Ганжур и др.

Эксперимент с прототипом жидко-криптонного
калориметра на пучке меченых фотонов

Budker INP 95-96

Ответственный за выпуск С.Г. Попов
Работа поступила 13.12 1995 г.

Сдано в набор 15.12. 1995 г.
Подписано в печать 15.12 1995 г.
Формат бумаги 60×90 1/16 Объем 2,6 печ.л., 2,1 уч.-изд.л.
Тираж 250 экз. Бесплатно. Заказ N 96

Обработано на IBM PC и отпечатано на
ротапринте ГНЦ РФ "ИЯФ им. Г.И. Будкера СО РАН",
Новосибирск, 630090, пр. академика Лаврентьева, 11.